Techniques to estimate fracture effectiveness when mapping low-magnitude microseismicity

Sherilyn Williams-Stroud, MicroSeismic Inc., Randal L. Billingsley, Tracker Resource Development, llc.*

Summary

Hydraulic fracture mapping by locating microseismic events related to rock fracturing is used to evaluate the effectiveness of the stimulation in low-permeability reservoirs. The geometry of the events is used to infer fracture orientation, particularly in the case where events line up along an azimuth, or have a planar distribution in 3 dimensions. When the induced the microseismic events have a low signal-to-noise ratio (either due to low magnitude or propagation effects) their locations can have a high degree of uncertainty. Low signal-to-noise events are not as accurately located in the reservoir, or are not detected at all, so that the extent of fracture stimulated reservoir may be underestimated. In the Bakken Formation of the Williston Basin, we combine geological analysis with process-based and stochastic fracture modeling to build multiple possible fracture model realizations. Specific parameters in the models can be modified while honoring a realistic range for each parameter in order to explore the range of uncertainty. Fracture flow properties generated from the fracture models are validated via history matching iterations. The validated fracture models, in turn, provide a means to calculate a geometrically-constrained volume of rock and fracture permeability that can be used for estimating production. This paper presents a methodology for deciding which fracture parameters to vary (the high sensitivity parameters) in order to minimize the number of realizations that need to be generated during the model conditioning phase of a reservoir simulation program.

Introduction

The Middle Bakken oil reservoir has proven to be a challenge for microseismic mapping. The apparent low anisotropy of the regional stress in the Williston Basin, the depth of the Bakken reservoir, and the average thickness of less than 100 feet in many productive fields may explain the low magnitudes of the induced microseismic events. Large vertical velocity/density variations within the basin fill also contribute to the acoustic challenge. Small magnitude events at depth result in low signal-to-noise ratio of microseismicity generated during hydraulic fracture stimulations monitored at the surface. The Bakken formation is also naturally fractured, so it is likely that the hydraulic fracture treatment reactivates existing fractures, rather than create new fractures. Stimulation of existing fracture networks is well documented in the literature in the Barnett Shale, for instance (Gale, 2007), and source mechanism analysis of hydraulic fracturing in reservoirs with strong microseismic energy show fracturing behavior that confirms complex failure behavior along existing fracture networks in response to the pressure changes induced by the stimulation (Eisner, 2010.). When natural fracture networks are stimulated by the hydraulic fracturing treatment, the resulting diffuse clouds of events do not provide enough information to infer fracture directions. In addition, the low stress anisotropy in the Williston Basin allows stimulation of a wider range of fracture orientations than in basins where the differential stress is much higher. We use the geologic setting and wellbore data to develop models for fracture orientation and length.

The relatively flat, gently dipping sedimentary bedding in the Williston Basin belies its structural complexity. Salt collapse features, faulting and subtle structural roll-overs influence trap formation. Basement faulting in the basin has been reactivated by tectonic activity subsequent to deposition of the oil-rich sedimentary sequence. A number of workers have used lineament analysis in the Williston Basin to identify structural trends that delineate structures and producing zones in the basin (Thomas, 1974, Gerhard et al, 1982). Figure 1 shows shaded-relief elevation in the area of the treatment well with two primary orientations of linear trends. Faulting in the basin is steeply dipping to vertical, and major structures are present on the surface that indicate left-lateral displacement upon reactivation. Although measurements of maximum horizontal stress are often unreliable, some data sources indicate a NE azimuth (Heidbach et al, 2008).

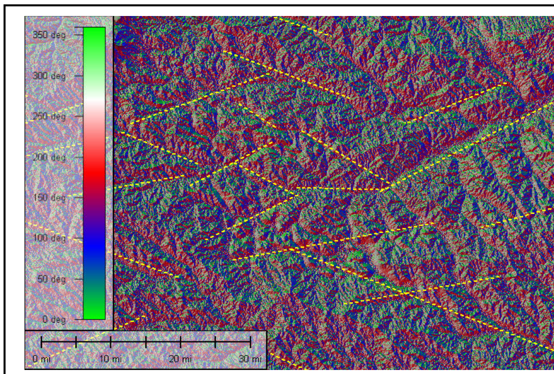

Figure 1. Shaded elevation view of the well area. View is colored by slope orientation (vertical scale bar) to highlight lineament directions. Distance on horizontal scale bar is 40 miles.

The prominence of the Brockton-Froid fault zone in the eastern Montana part of the Williston Basin suggest the E-EW oriented lineaments are most recently active as strike slip faults. This interpretation is supported by the orientation of conductive natural fractures identified in image logs from a neighboring well. (Figure 2). Conductive fracture orientations and densities vary along the wellbore and, in general, mirror the orientations that can be identified in the large scale lineaments.

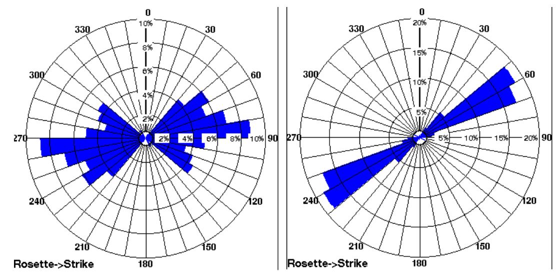

Figure 2. Rose diagram of strikes of conductive fractures identified in image log through middle Bakken (latch 2, 15,675'- 20,223' MD) (left), and rose strike of conductive fractures from latch 1 (13,500-16,095' MD)(right)

Methodology

Difficulties related to monitoring microseismicity in the Bakken Formation in the Williston Basin are commonly experienced by monitoring companies regardless of the acquisition method. An experiment undertaken in fall 2007 by a consortium of 7 operators, 3 microseismic monitoring service companies and Lawrence Berkeley Labs was designed to evaluate different acquisition methods and determine the most effective approach to monitoring Bakken hydraulic fracture stimulations (North Dakota Oil and Gas Research Council report G-015-028). Two different types of buried arrays were deployed on the project, one downhole array in a horizontal well, and a surface based array of the same type used to acquire the data for this study. The two buried arrays detected no microseismic events, likely due to the small number of geophone stations and their distance from the deep reservoir. The downhole monitoring produced a sparse set of events, consisting of the relatively small number of events that could be accurately located using the P an S wave arrivals, and with a large vertical location uncertainty. Approximately 800 events were imaged from the surface based radial array of geophones. Diffuse trends in the event clouds formed in orientations interpreted to be related to the regional lineaments in the Williston Basin.

Microseismic data were collected during the stimulation treatment of a well in the Bakken Formation in west-central North Dakota using a surface-based monitoring method. An array of geophones was laid out in a radial pattern around the treatment well, and consisted of 1336 stations of 24 geophones. Eight stages were treated in the well using a "ball drop" completion method, with a total of 18 hours of data recorded. Microseismic events induced by the hydraulic fracturing were located by a beamforming process, which is essentially a one-way depth migration. A layered velocity model was calibrated using a string shot as the calibration source.

More than 300 microseismic events were identified and located with their relative energy. Figure 3 shows the result of the final processed events from the study well. Events are colored by stage and sized by relative energy. In 3 of the 8 stages a fairly well defined, but diffuse trend can be seen parallel to a NNE azimuth. Stage 1 also shows a SSE azimuth trend of events.

A geocellular model was populated with the events, using their locations and relative energy as a fracture probability within the model. Six events with enough energy that they were visible in the raw seismic traces were recorded during the stimulation treatment, but the energy from these events was not high enough to invert these events for source their mechanisms. In cases such as these where the event energy is low, we use a probabilistic approach to generating the fractures. The lineament analysis and natural fracture orientations from the image log are used to constrain the orientations of the modeled fractures. Using an average strike of 59 degrees, multiple realizations of fractures are generated with different length distributions and orientation distributions. A third parameter that was varied for the fracture realization was the fracture probability. The observed amplitude of a microseismic event is proportional to seismic moment of the event. Thus we have calibrated stacked amplitudes of the detected microseismic events to seismic moments. The values of stacked amplitudes are used directly as the P32 (fracture area per volume) parameter, and different functions were applied to the amplitude values to test their effect on the fracture probability distribution. When the seismic moment can be calculated directly, the size of the fracture surface can be calculated from the following relationship:

$$M_0 = \mu S d \qquad (1)$$

Where μ = rigidity, S = fracture area, and d = displacement. Varying the P32 fracture intensity input parameter parameter also changes the size distribution of the generated fractures relative to the magnitude of the event energy. This methodology is a way to model the relationship of the seismic moment to the fracture size, when the full source mechanism is not available.

The fracture network generated from one of the amplitude/fracture length distribution relationships is shown in figure 4. The locations of higher signal-to-noise events that served as a fracture probability constraint in the input parameter are locations of high fracture intensity in the resulting fracture model. The small dots visible in the image with the fractures show the locations where events were processed, but because of their low amplitude, not all of these locations resulted in fractures being generated. The random seed used to generate a fracture set can be changed to create a new fracture sets that are statistically equivalent but have a slightly different fracture distribution so that different low amplitude event locations generate fractures.

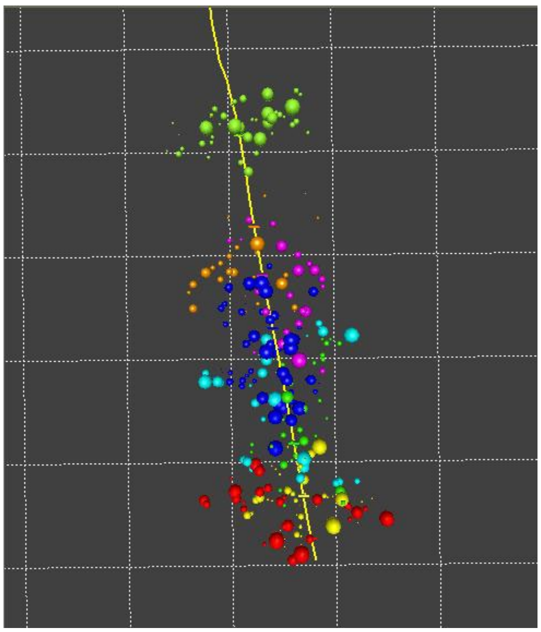

Figure 3. Microseismic events detected from 8 stages of hydraulic fracture stimulation. Events are colored by stage and sized by relative amplitude. Grid cells are 2000 feet square.

Fracture Characterization

Another potential uncertainty to be tested is the presence of a second fracture set with NW strike orientation, as could be interpreted from the event trends shown in Figure 3 and in the regional lineaments (Fig. 1). NW striking fractures in a stress field with maximum horizontal stress NE azimuth may be less likely to be activated by the fracture stimulation (Zoback, 2007). However, with low stress anisotropy, they may make important contributions to the overall permeability. Testing the impact on permeability of a third fracture set with NW strike is simplified by comparing output properties generated with and without this set.

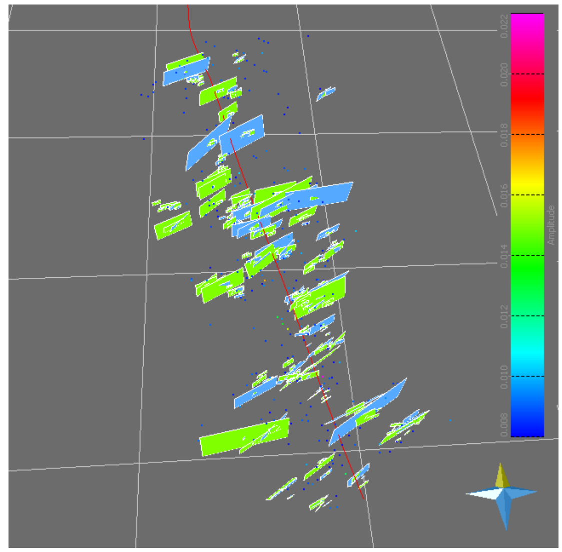

Figure 4. Fractures generated from microseismic event locations and relative energy. Two fracture sets are visible, one dipping steeply to the S-SE and the other dipping steeply to the N-NW. Dots around the wellbore are locations of low amplitude microseismic events where fractures were not generated.

The flow properties generated from the fracture models are calculated from the total area of fractures within each cell of the geocellular grid. Fracture aperture is assigned by using a relationship to the fracture length, and the permeability tensor is calculated using a weighted average of these three properties. If a generated fracture extends beyond the boundaries of a cell, it is clipped to the cell boundaries so that only the area portion of the fracture contained within the cell is used to calculate the fracture porosity volume. This value of fracture porosity, or storativity, is output to the geocellular grid, and is given by

$$\boldsymbol{Porosity} = \frac{\sum_{\boldsymbol{polygons}} \boldsymbol{V_{polygon}}}{\boldsymbol{V_{cell}}} \qquad (2)$$

where the volume of an individual polygon is equal to its surface area multiplied by its aperture. The total cell volume defining the stimulated reservoir contains an associated total storage value related to the fracture volume as defined above, and can serve as an estimate for a minimum drained volume related to the stimulation.

Analysis of how the fracture flow property output varies with changes in particular input parameters shows which input parameter the model is most sensitive to. Because image loges and core can only intersect a small area of the fractures, one of the highest uncertainties in a fracture model constrained by data from these sources is the length. The chart in figure 5 shows output properties generated by changing the fracture length distribution only. The chart shows that the output permeability is highly sensitive to the length distribution.

The total volume of stimulated reservoir is dependent on the fracture model used to calculate the fracture flow properties. The distribution of fracture permeability calculated from the fracture model in figure 6 shows how the fracture sizes and locations determine the high permeability streaks in the reservoir model. The volume of reservoir that may have enhanced fracture permeability is shown, with all cells containing no additional fracture flow properties turned off in the display. The resulting volume of stimulated reservoir is also sensitive to the input parameters used to generate the fracture model, so multiple realizations will generate different extents and volumes of stimulated reservoir. The different realizations can be validated via history matching, but the process is streamlined by determining the sensitive input parameters. The number of realizations that need to be generated for history matching is reduced by generating only models where the sensitive parameters are changed.

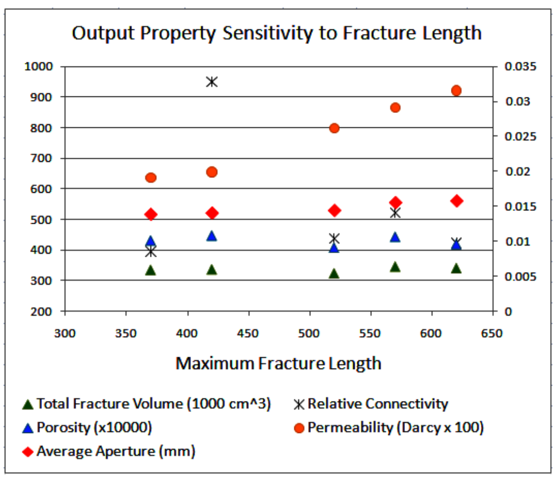

Figure 5. Output property sensitivity to input parameters for fracture network model. Output fracture permeability is highly sensitive to changes in the distribution of fracture lengths in the input parameters.

Conclusions

We have presented in this paper a methodology for generating fracture models from microseismic events in reservoirs that generate low- seismic energy during the stimulation treatment resulting on low signal-to-noise events. The resulting event locations may have a high degree of uncertainty, so that the impact of the fracture uncertainty needs to be investigated in order to determine the extent of reservoir stimulation. The location and size uncertainty are quantified by generating multiple realizations based on geological parameters that are known about the reservoir such as fracture orientation from image logs, or structural trends. In the output, the sensitive parameters are identified before sending the model to reservoir simulation so that the number of models that need to be generated is reduced. Rather than generating many models using a Monte Carlo approach, a small number of models can be generated where only the sensitive parameters are varied. The fracture models can then be validated via history matching, so that more accurate estimates of the total volume of stimulated reservoir can be calculated in order to determine reserves and guide infill drilling programs.

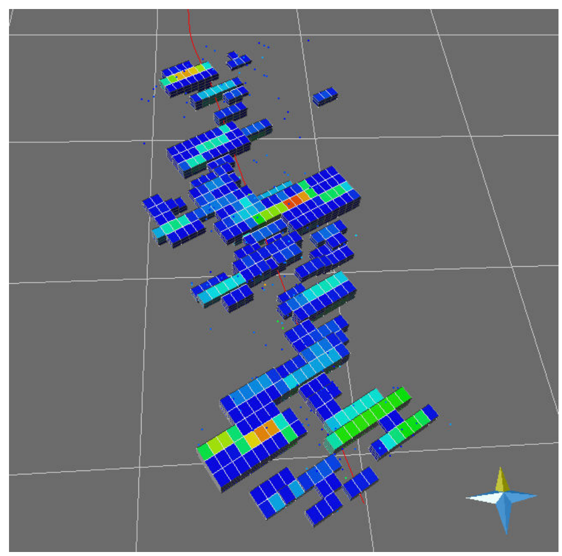

Figure 6. Geocellular volume showing permeability output properties calculated from fractures. Warm colors are high permeability cells. All cells in the model without fracture permeability are turned off in the display

Acknowledgements

The authors wish to thank Michael Thornton and Leo Eisner for their helpful and critical reviews of this abstract, and William Barker for geophysical support in the microseismic data processing and interpretation of the monitoring results. We also wish to thank Tracker Resource Development LLC for release of this data set for publication.

EDITED REFERENCES

Note: This reference list is a copy-edited version of the reference list submitted by the author. Reference lists for the 2010 SEG Technical Program Expanded Abstracts have been copy edited so that references provided with the online metadata for each paper will achieve a high degree of linking to cited sources that appear on the Web.

REFERENCES

Eisner, L., S. C. Williams-Stroud, A. Hill, P. Duncan, and M. Thornton, 2010, Beyond the Dots in the Box: Microseismicity-Constrained Fracture Models for Reservoir Simulation: The Leading Edge, **29**, no. 326, doi: 10.1190/1.3353730.

Gale, J. F., R. M. Reed, and J. Holder, 2007, Natural Fractures in the Barnett Shale and their Importance for Hydraulic Fracture Treatments: AAPG Bulletin, **91**, no. 4, 603–622, doi:10.1306/11010606061.

Gerhard, L. C., S. B. Anderson, J. A. Lefever, and C. G. Carlson, 1982, Geological Development, Origin, and Energy Mineral Resources of Williston Basin, North Dakota: AAPG Bulletin, **66**, no. 8, 989–1020.

Heidbach, O., M. Tingay, A. Barth, J. Reinecker, D. Kurfeß, and B. Müller, 2009, The World Stress Map based on the database release, equatorial scale 1:46,000,000: Commission for the Geological Map of the World, doi:10.1594/GFZ.WSM.Map2009.

North Dakota Oil and Gas Research Program Technical Summmary, 2009, G-015-029 Hydraulic Fracturing and Microseismic Monitoring Project: Bakken Research Consortium.

Thomas, G. E., 1974, Lineament-Block Tectonics: Williston-Blood Creek Basin: AAPG Bulletin, **58**, no. 7, 1305-1322

Zoback, M., 2007, Reservoir Geomechanics: Cambridge University Press.